Electronic Supplementary Material (ESI) for Journal of Materials Chemistry C.

Supporting Information

Optimized physical properties of [001]-textured (Na, K)NbO_3-based lead-free piezoceramics for high power piezoelectric energy harvester

Seok-June Chae, Seung-Hyun Kim, In-Su Kim, Geun-Soo Lee, Seok-Jung Park and Sahn Nahm*

Department of Materials Science and Engineering, Korea University, 145 Anam-ro, Seongbuk-gu, Seoul 02841, Republic of Korea

*Corresponding author. E-mail: snahm@korea.ac.kr

1. Fabrication of $NaNbO_3$ (NN) templates, and measurement of the physical properties of the piezoceramics and the output properties of the piezoelectric energy harvester

NN templates were used to texture $NK(N_{1-x}S_x)$-CZ-BAZ piezoceramics; the topochemical microcrystal conversion and molten salt method were used to fabricate the NN templates [1, 2]. Na_2CO_3, Nb_2O_5, and Bi_2O_3 (≥ 99.9%, High Purity Chemicals, Japan) were mixed by ball milling for 12 h and then heated in molten NaCl (≥ 99.9%, High Purity Chemicals, Japan) at 1150 ℃ for 6 h to produce the $Bi_{2.5}Na_{3.5}Nb_5O_{18}$ (BNN) template. The NN templates were fabricated using a topochemical microcrystal conversion reaction between BNN and Na_2CO_3 at 975 ℃ for 6 h in molten NaCl. The weight ratio of the reacting oxide chemicals and salt in all reactions was maintained at 1:1.5. The NN template had a homogeneous perovskite phase without any secondary phases (Fig. S1(a)). The NN template was 12 × 12 × 1.0 μm with an aspect ratio of approximately 12 (Fig. S1(b)), confirming that the NN template was successfully fabricated from the BNN template.

The crystal structures of the samples were determined using X-ray diffraction (XRD; XRD-6100, Shimadzu, Kyoto, Japan) using Cu *Kα* radiation. The XRD patterns of the piezoelectric ceramics were analyzed using Rietveld refinement using the FullProf suite program to determine the detailed crystal structures of the samples. Field-emission scanning electron microscopy (SEM; S-4800, Hitachi, Tokyo, Japan) was used to study the microstructures of the samples. Additionally, field-emission transmission electron microscopy (TEM; Spectra 300 TEM, Thermo Fisher Scientific, USA) was used to investigate the domain structure of the ceramics, and the TEM samples were prepared using focused ion-beam milling (Helios G4 UC, Thermo Fisher Scientific, USA). The densities of the specimens were measured using Archimedes' principle. The unit cell volume of the specimen was obtained by determining its crystal structure by Rietveld analysis. The unit cell

volume was then used to calculate the theoretical densities of the specimens, which are listed in Table S1. The piezoceramics were coated with silver electrodes and poled in silicone oil at room temperature (RT) using a DC electric field of 4 kV/mm for 30 min. The d_{33} value was measured using a d_{33} meter (ZJ-4B, Academia Sinca, China). Further, the $\varepsilon^T_{33}/\varepsilon_0$ values were measured at various temperatures using an impedance analyzer (HP 4194A, Agilent Technologies, Santa Clara, CA, USA). Polarization-electric field (*P*-*E*) hysteresis loops were detected using a ferroelectric tester (aixACCT Systems, Aachen, Germany). The strain-electric field (*S*-*E*) curves were measured using a laser displacement sensor (aixACCT Systems, Aachen, Germany) at 1.0 Hz in silicone oil. To investigate the fatigue properties, an electric field of 1.0 kV/mm, which is similar to the coercive electric field (E_C) of piezoceramics, was continuously applied during cycling at a frequency of 100 Hz.

Cantilever-type PEHs were produced using the [001]-textured NK($N_{1-x}S_x$)-CZ-BAZ piezoceramics ($0.0 \leq x \leq 0.1$). Vibrational mechanical energy was applied to the PEH using an artificial exciter (Type 4809, Brüel & Kjaer, Nærum, Denmark) with a vibrational acceleration of 9.8 m/s^2 (1.0 g). COMSOL (COMSOL, Burlington, MA, USA) was used to simulate the mechanical stress developed in the PEH. The output voltage of the PEH was measured using a digital oscilloscope (DPO3034; Tektronix, Beaverton, OR, USA). The current and electric power outputs of the PEHs were obtained at different electric load resistances (R_L) and external vibrational frequencies using the measured voltage outputs.

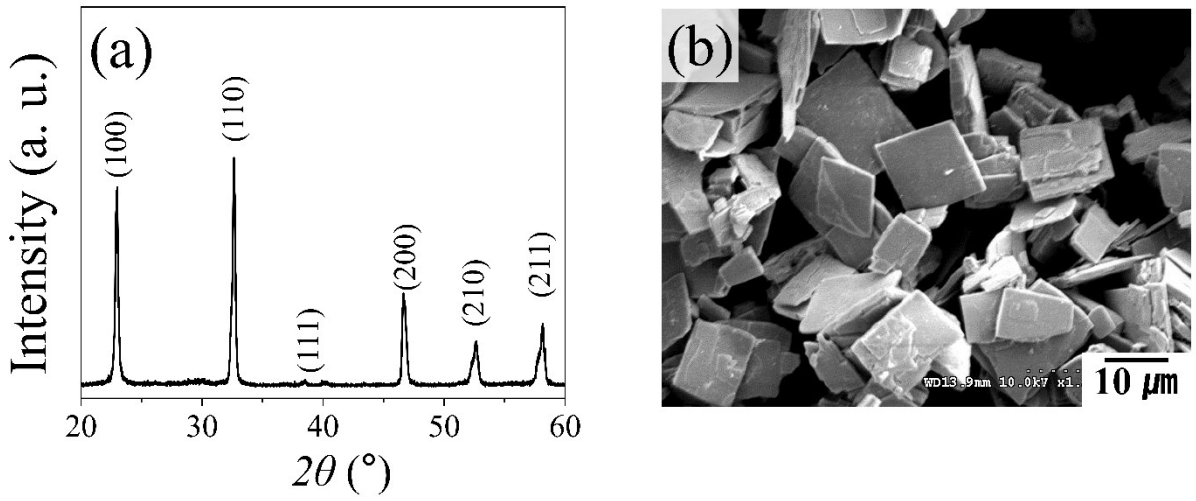

Fig. S1 (a) XRD pattern and (b) SEM image of the NN templates

Table S1. Actual and theoretical densities of the specimens.

x	0.00	0.01	0.02	0.03	0.04	0.05
Theoretical density (g/cm^3)	4.843	4.872	4.881	4.902	4.912	4.914
Actual density/Untextured (g/cm^3)	4.654	4.664	4.640	4.635	4.615	4.606
Actual density/Textured (g/cm^3)	4.557	4.538	4.543	4.538	4.543	4.547
x	0.06	0.07	0.08	0.09	0.10	
Theoretical density (g/cm^3)	4.915	4.919	4.929	4.948	4.950	
Actual density/Untextured (g/cm^3)	4.567	4.601	4.586	4.577	4.577	
Actual density/Textured (g/cm^3)	4.557	4.538	4.518	4.509	4.499	

2. XRD diffraction patterns of the NK($N_{1-x}S_x$)-CZ-BAZ piezoceramics ($0.0 \leq x \leq 0.1$)

Fig. S2 shows XRD patterns of the NK($N_{1-x}S_x$)-CZ-BAZ piezoceramics ($0.0 \leq x \leq 0.1$) sintered at 1090 °C for 6 h. All samples exhibited a homogeneous perovskite structure without secondary phases. Therefore, it was considered that the NK($N_{1-x}S_x$)-CZ-BAZ piezoceramics were well densified at 1090 °C. The shape of the XRD peaks at approximately 45.5° changed with an increasing x, indicating that the crystal structure of the sample changed with an increasing x. However, it is difficult to clearly identify the crystal structure using the normal XRD patterns. Therefore, Rietveld analyses were conducted on the XRD patterns of the NK($N_{1-x}S_x$)-CZ-BAZ piezoceramics ($0.0 \leq x \leq 0.1$), as shown in Fig. 2(a)–(e) of the main document. The crystal structure of the NK($N_{1-x}S_x$)-CZ-BAZ piezoceramics ($0.0 \leq x \leq 0.1$) changed from the *O*-*T* mixed structure to the *R*-*O*-*T*, *R*-*T*, and *R*-*T*-*C* mixed structures.

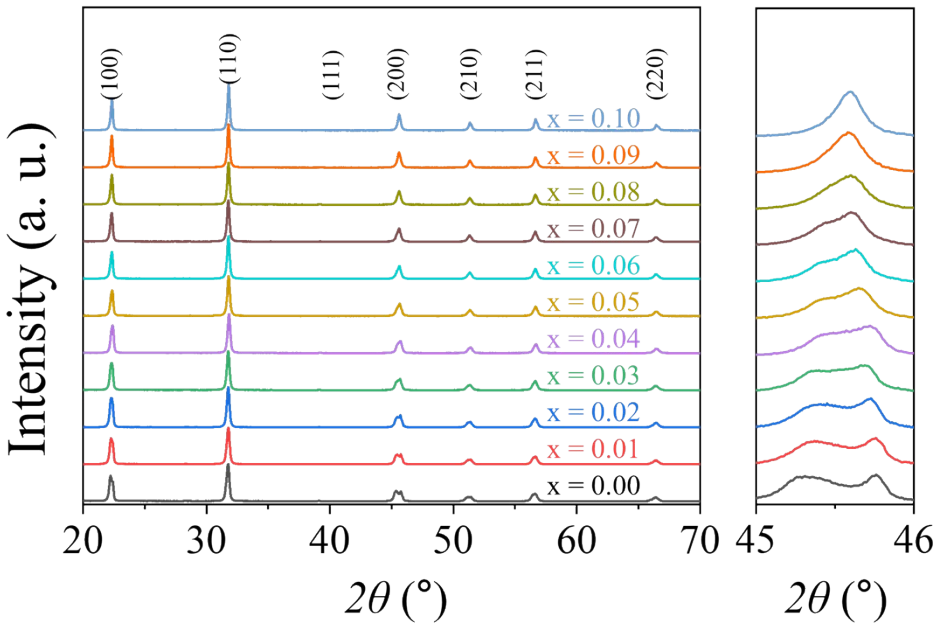

Fig. S2 XRD patterns of the NK($N_{1-x}S_x$)-CZ-BAZ piezoceramics with $0.0 \leq x \leq 0.1$ sintered at 1090 °C for 6 h

3. $\varepsilon^{T}_{33}/\varepsilon_0$ versus temperature curves of the NK($N_{1-x}S_x$)-CZ-BAZ piezoceramics

Fig. S3(a)–(f) show the $\varepsilon^{T}_{33}/\varepsilon_0$ versus temperature curves of the NK($N_{1-x}S_x$)-CZ-BAZ piezoceramics ($0.01 \leq x \leq 0.09$), and the inset shows the $\varepsilon^{T}_{33}/\varepsilon_0$ versus temperature curve of the corresponding sample at -50–400 °C. The T_C of the x = 0.01 sample was approximately 313 °C (Fig. S3(a)) and it decreased to approximately 94 °C with an increasing x for the sample with x = 0.09 (Fig. S3(f)). $T_{O\text{-}T}$ decreased and $T_{R\text{-}O}$ increased with an increasing x, and they merged as $T_{R\text{-}O\text{-}T}$ at approximately 45 °C in the x = 0.07 sample (Fig. S3(e)). Finally, the temperature range in which the *O* phase is stable disappeared and $T_{R\text{-}O\text{-}T}$ changed to $T_{R\text{-}T}$, as shown in Fig. S3(f). Additionally, the T_C and $T_{O\text{-}T}$ (or $T_{R\text{-}O\text{-}T}$) peaks widened with an increasing x. Furthermore, the T_C and $T_{O\text{-}T}$ (or $T_{R\text{-}O\text{-}T}$) peaks shifted to a high temperature with an increasing frequency, and the difference in the temperature (ΔT) between the maximum and minimum frequencies also increased with an increasing x. Therefore, it is suggested that the relaxor properties for the NK($N_{1-x}S_x$)-CZ-BAZ piezoceramics ($0.01 \leq x \leq 0.09$) increased with an increasing Sb^{5+} content.

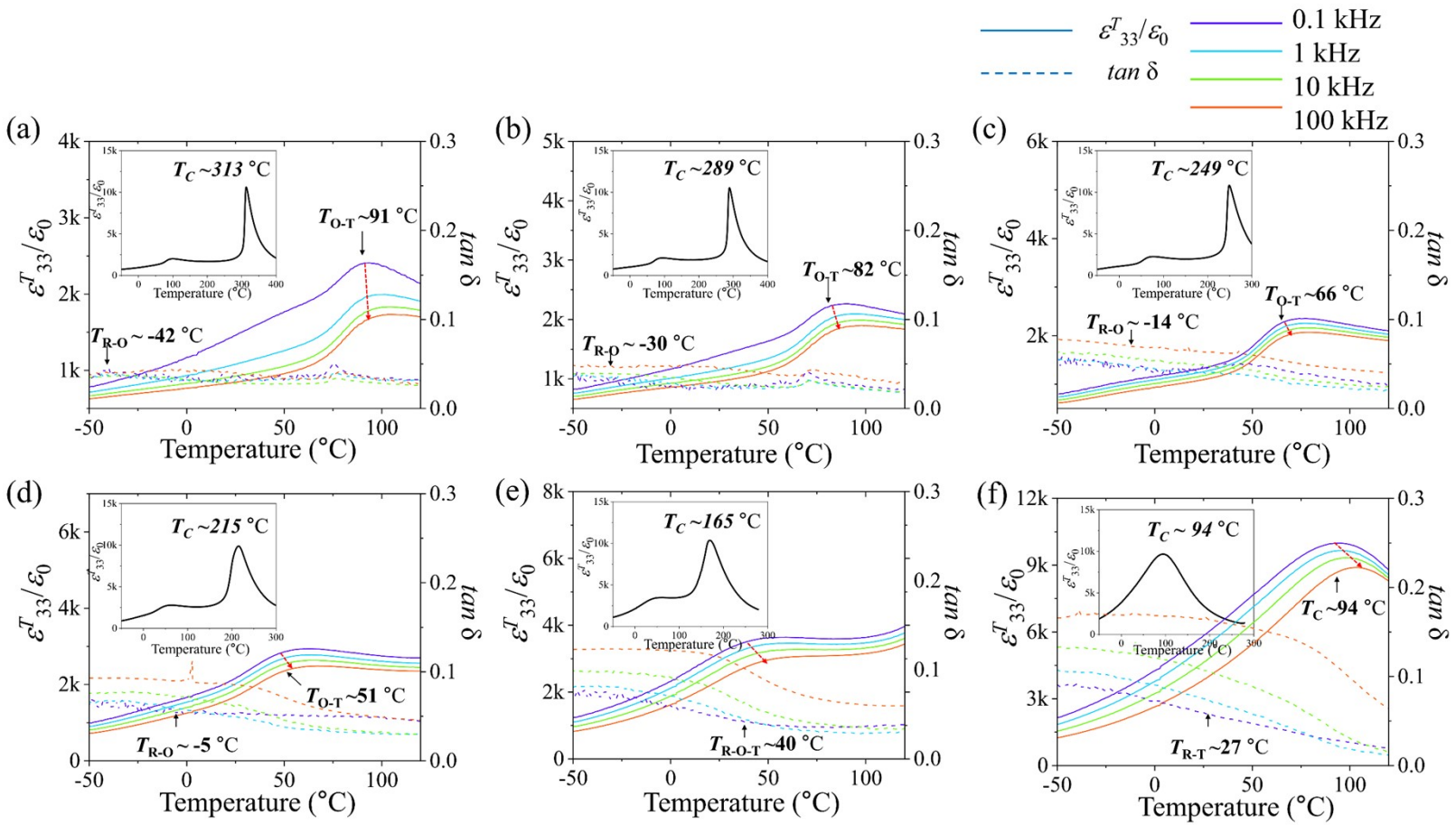

Fig. S3 $\varepsilon^T_{33}/\varepsilon_0$ versus temperature curves of the NK($N_{1-x}S_x$)-CZ-BAZ piezoceramics with (a) x = 0.01, (b) x = 0.02, (c) x = 0.04, (d) x = 0.05, (e) x = 0.07 and (f) x = 0.09.

4. SEM images of the untextured NK($N_{1-x}S_x$)-CZ-BAZ piezoceramics ($0.0 \leq x \leq 0.1$)

The microstructures of the untextured NK($N_{1-x}S_x$)-CZ-BAZ piezoceramics ($0.0 \leq x \leq 0.1$) were investigated using SEM; Fig. S4(a)–(g) show SEM images of the thermally-etched surfaces of the samples. All the samples exhibited a dense microstructure. The holes shown in the samples were possibly formed during the preparation of the SEM samples. Therefore, all the samples were well densified. The $0.0 \leq x \leq 0.03$ samples exhibited large grains with an average grain size of 40 μm (Fig. S4(a)–(c)). The grain size decreased when x exceeded 0.03, and the average grain size of the $x = 0.1$ sample was approximately 15 μm, as shown in Fig. S4(g). Therefore, the grain size of the untextured NK($N_{1-x}S_x$)-CZ-BAZ piezoceramics ($0.0 \leq x \leq 0.1$) decreased when a large amount of the Sb^{5+} ions was added to the samples.

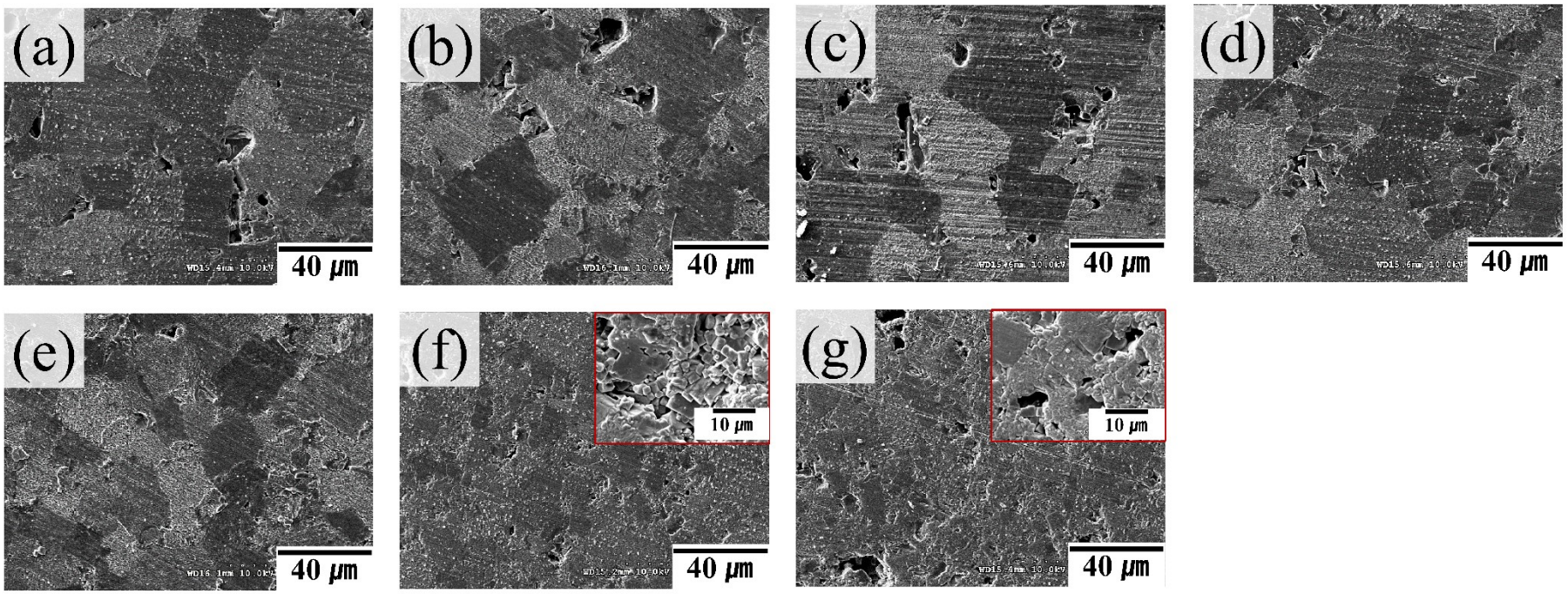

Fig. S4 SEM images of the NK($N_{1-x}S_x$)-CZ-BAZ piezoceramics with (a) x = 0.0, (b) x = 0.01, (c) x = 0.03, (d) x = 0.05, (e) x = 0.07, (f) x = 0.09, and (g) x = 0.1

5. SEM images of the textured NK($N_{1-x}S_x$)-CZ-BAZ piezoceramics ($0.0 \leq x \leq 0.1$)

The microstructures of the [001]-textured NK($N_{1-x}S_x$)-CZ-BAZ piezoceramics ($0.0 \leq x \leq 0.1$) were investigated, and Fig. S5(a)–(f) show SEM images of the fractured surface of the samples. Most of the grains of the samples were well aligned along the [001] direction. All the samples exhibited large grains with an average grain size of approximately 40 μm. Therefore, [001] texturing aligned the grains along the [001] direction and increased the grain size. Note that all samples exhibited various holes and some of them may have been produced during the preparation of the SEM samples. However, some of holes, as indicated by the arrows in Fig. S5(a)–(f), could be formed by the dissolution of the NN templates into the matrix of the samples. However, further investigation is required to clearly understand the formation mechanism of these holes.

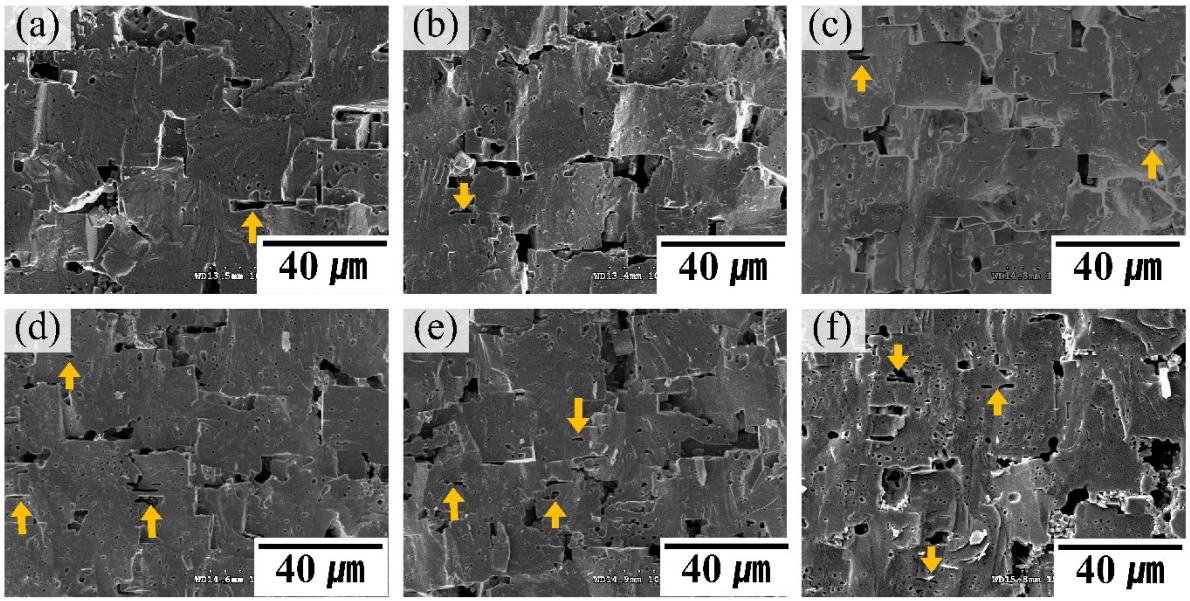

Fig. S5 SEM images of the textured NK($N_{1-x}S_x$)-CZ-BAZ piezoceramics with (a) x = 0.0, (b) x = 0.03, (c) x = 0.05, (d) x = 0.07, (e) x = 0.09, and (f) x = 0.1

6. Rietveld refinement of [001]-textured NK($N_{1-x}S_x$)-CZ-BAZ piezoceramics

Rietveld refinement was conducted on the XRD patterns of the [001]-textured NK($N_{1-x}S_x$)-CZ-BAZ piezoceramics with $0.0 \leq x \leq 0.1$ sintered at 1090 °C for 6 h, as shown in Fig. S6(a)–(e). Fig. S6(f) shows the proportions of the *R*, *O*, and *T* structures of the samples. Various physical parameters obtained from the Rietveld refinement are listed in Table S2. The textured x = 0.0 sample exhibited an *O*-*T* mixed structure composed of the *Amm2 O* (90.77%) and *P4mm T* structures (9.3%) (Fig. S6(a)). The x = 0.01 sample exhibited an *R*-*O*-*T* mixed structure consisting of the *R3m R*, (6.3%), *Amm2 O* (82.3%), and *P4mm T* structures (11.4%) (Fig. S6(b)). However, since the proportion of the *O* structure is significantly larger than those of the *T* structure of the x = 0.0 sample and the *R*-*T* structure of the x = 0.01 sample, the structure of the samples (x = 0.0 and x = 0.01) could be similar to the *O* structure. The proportion of the *O* structure decreased and those of the *R* and *T* structures increased with an increasing x. In particular, the x = 0.07 sample had an ideal *R*-*O*-*T* structure, in which each structure had a similar proportion of approximately 33%, as shown in Fig. S6(c). Since the *O* structure in the x = 0.09 sample disappeared, this sample had an *R*-*T* mixed structure, as shown in Fig. S6(d)). Finally, the cubic (*C*) structure was newly developed in the x = 0.1 sample owing to the large decrease in T_C (Fig. S6(e)). Therefore, the crystal structure of the [001]-textured NK($N_{1-x}S_x$)-CZ-BAZ piezoceramics ($0.0 \leq x \leq 0.1$) changed from the *O*-*T* mixed structure to the *R*-*O*-*T*, *R*-*T*, and *R*-*T*-*C* mixed structures. Furthermore, the crystal structures of the textured samples were very similar to those of the untextured samples.

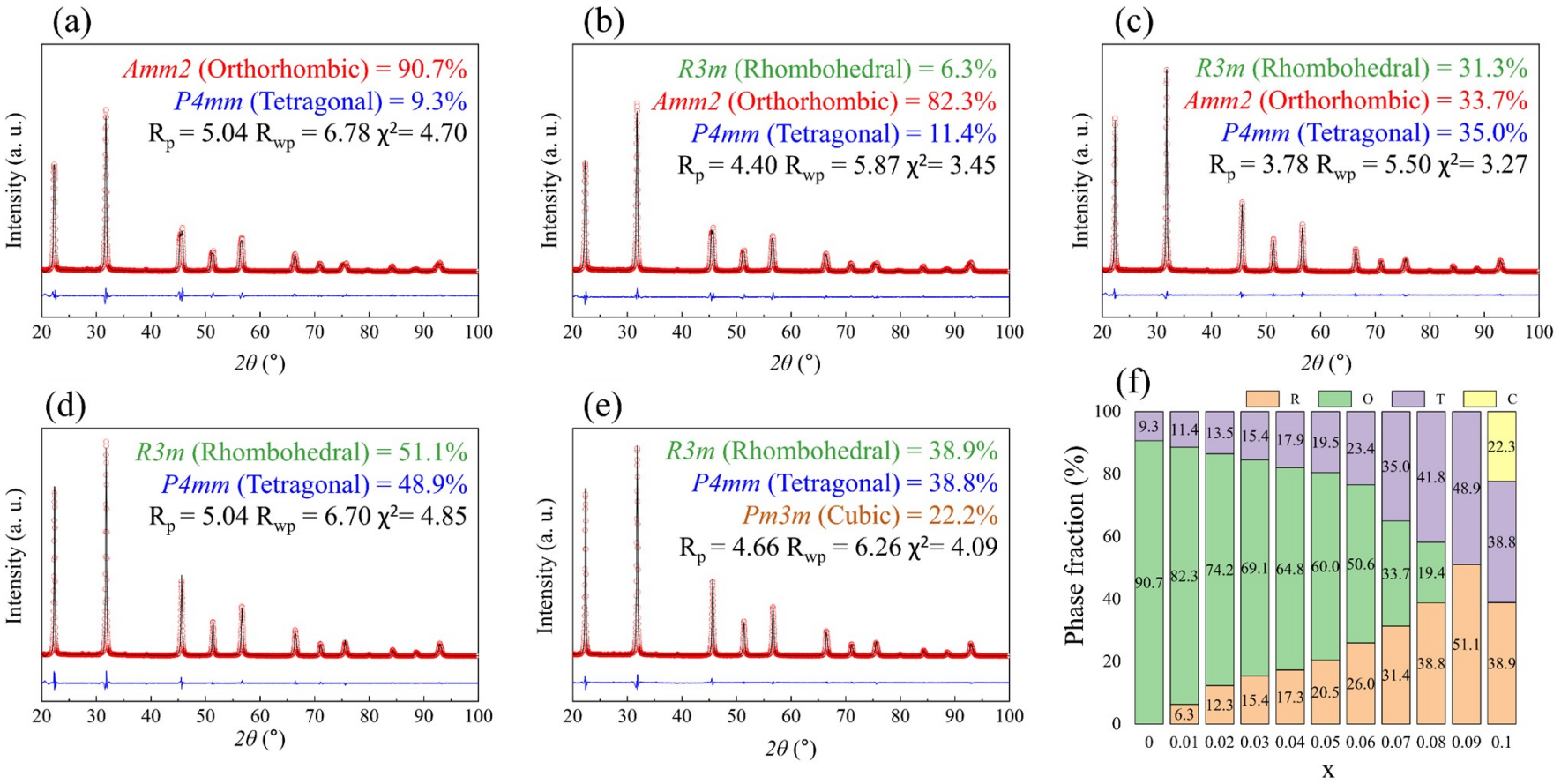

Fig. S6 Rietveld refinement of the XRD patterns of the textured NK($N_{1-x}S_x$)-CZ-BAZ piezoceramics with (a) x = 0.0, (b) x = 0.01, (c) x = 0.07, (d) x = 0.09, and (e) x = 0.1. (f) Proportions of *R*, *O*, and *T* structures in the NK($N_{1-x}S_x$)-CZ-BAZ piezoceramics.

Table S2. Structural properties of the [001]-textured NK($N_{1-x}S_x$)-CZ-BAZ piezoceramics ($0.0 \leq x \leq 0.1$) analyzed using the Rietveld refinement method.

Sb	Phase structure	Phase fraction (%)	Lattice parameters				R_p (%)	R_{wp} (%)	χ^2
			a (Å)	b (Å)	c (Å)	α, β, γ			
0.00	*O-T*	90.7 (Amm2)	3.9621 (3)	5.6545 (4)	5.6589 (4)	α = β = γ = 90°	5.04	6.78	4.70
		9.3(P4mm)	3.9751 (3)	3.9751 (3)	3.9764 (3)	α = β = γ = 90°			
0.01	*R-O-T*	6.3 (R3m; H)	5.6635 (9)	5.6635 (9)	6.9954 (24)	α = β = 90°, γ = 120°	4.40	5.87	3.45
		82.3 (Amm2)	3.9655 (3)	5.6503 (4)	5.6535 (4)	α = β = γ = 90°			
		11.4 (P4mm)	3.9725 (3)	3.9725 (3)	3.9819 (3)	α = β = γ = 90°			
0.07	*R-O-T*	31.3 (R3m; H)	5.6250 (1)	5.6250 (1)	6.8996 (3)	α = β = 90°, γ = 120°	3.78	5.50	3.27
		33.7 (Amm2)	3.9690 (3)	5.6374 (3)	5.6405 (3)	α = β = γ = 90°			
		35.0 (P4mm)	3.9756 (1)	3.9756 (1)	3.9850 (1)	α = β = γ = 90°			
0.09	*R-T*	51.1 (R3m; H)	5.6250 (1)	5.6250 (1)	6.8996 (3)	α = β = 90°, γ = 120°	5.04	6.70	4.85
		48.9 (P4mm)	3.9756 (1)	3.9756 (1)	3.9850 (1)	α = β = γ = 90°			
0.1	*R-T-C*	38.9 (R3m; H)	5.6250 (1)	5.6250 (1)	6.8996 (3)	α = β = 90°, γ = 120°	4.66	6.26	4.09
		38.8 (P4mm)	3.9690 (3)	5.6374 (3)	5.6405 (3)	α = β = γ = 90°			
		22.2 ($Pm\bar{3}m$)	3.9756 (1)	3.9756 (1)	3.9850 (1)	α = β = γ = 90°			

7. Relaxor properties of the textured NK($N_{1-x}S_x$)-CZ-BAZ piezoceramics

Fig. S7-1(a)–(f) show the changes in $1/(\varepsilon^{T}_{33}/\varepsilon_0)$ as a function of the temperature for the [001]-textured NK($N_{1-x}S_x$)-CZ-BAZ piezoceramics ($0.0 \leq x \leq 0.1$). The deviations of all the samples from the Curie–Weiss law, which is defined as $\Delta T_m = T_{dev} - T_m$, where T_m is the transition temperature and T_{dev} is the temperature at which $\varepsilon^{T}_{33}/\varepsilon_0$ begins to deviate from the Curie–Weiss law, were investigated [3–5]. The ΔT_m values of all the specimens are shown in Table S3. Moreover, the modified Curie–Weiss law can be expressed as Eq. (S1),

$$1/(\varepsilon^{T}_{33}/\varepsilon_0) - 1/\varepsilon_m = (T - T_m)^{\gamma}/C \quad \text{(S1)}$$

where γ and C are constants with $1 \leq \gamma \leq 2$ [6]. The γ of a normal ferroelectric material is close to 1.0. As γ approaches 2.0, the ferroelectric material has relaxor properties [6]. Fig. S7-2(a)–(f) and Table S3 present the γ values of the [001]-textured NK($N_{1-x}S_x$)-CZ-BAZ piezoceramics ($0.0 \leq x \leq 0.1$). The γ value of the x = 0.0 sample was approximately 1.22, and the x = 0.01 sample exhibited a similar γ value (1.34). Therefore, these samples were considered to be normal ferroelectric ceramics. The γ value increased with an increasing x, and the x = 0.1 sample had a large γ value of 1.92. Therefore, the relaxor properties increased with an increasing x, and the x = 0.1 sample exhibited the largest relaxor properties.

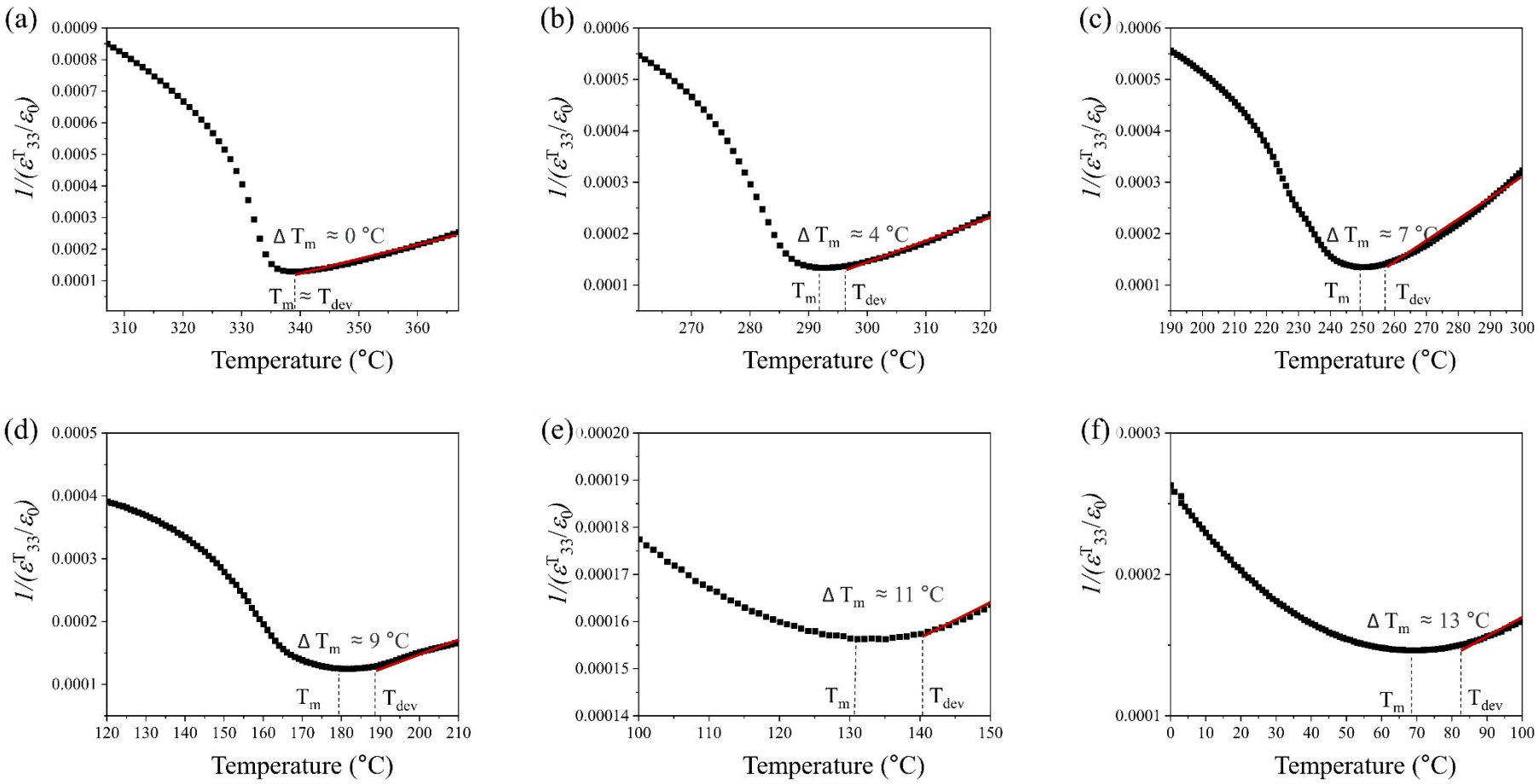

Fig. S7-1 Variations in the $1/(\varepsilon^T_{33}/\varepsilon_0)$ values for the textured NK($N_{1-x}S_x$)-CZ-BAZ piezoceramics with temperature: (a) x = 0.0, (b) x = 0.02, (c) x = 0.04, (d) x = 0.06, (e) x = 0.08, and (f) x = 0.1.

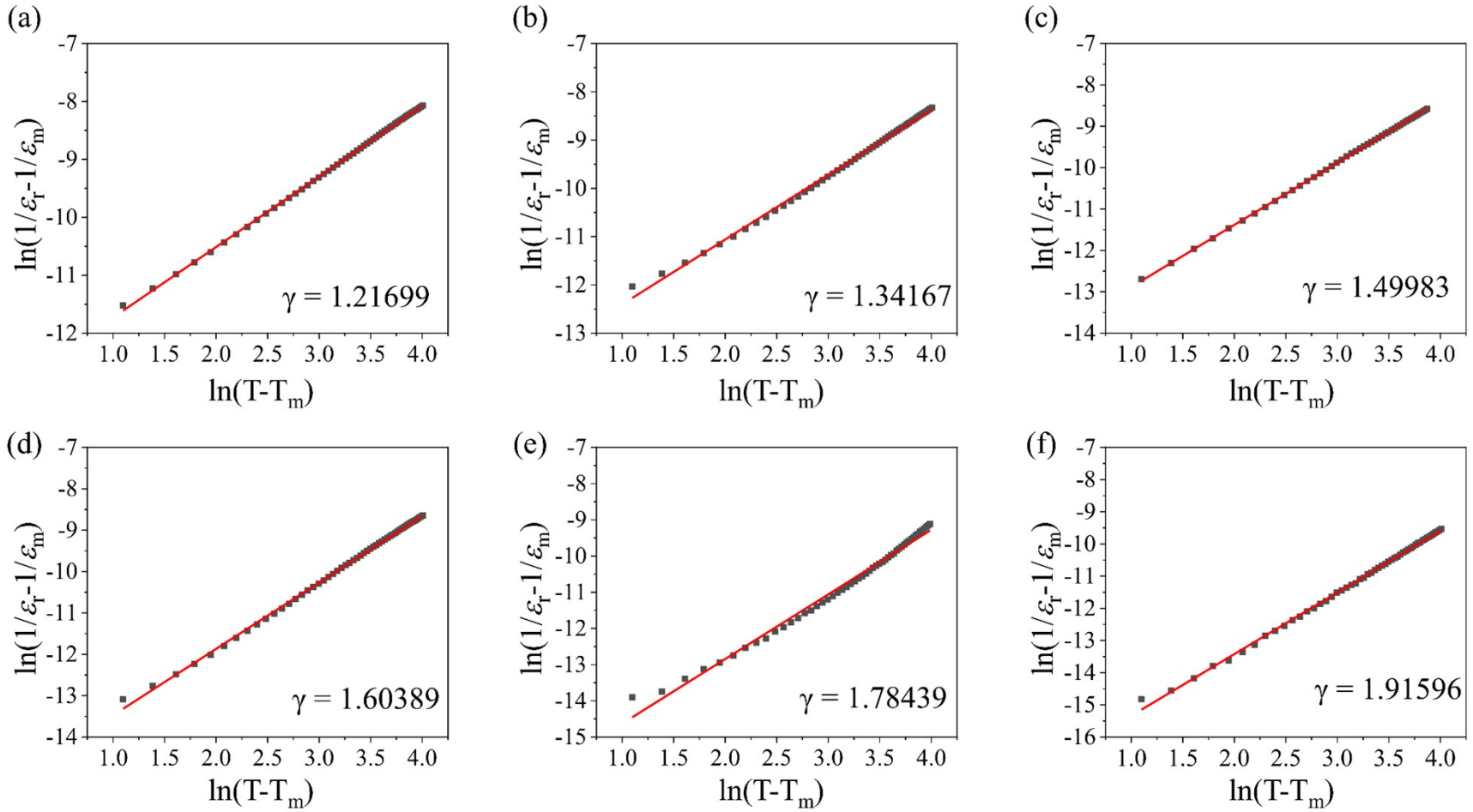

Fig. S7-2 ln $(1/\varepsilon_r - 1/\varepsilon_m)$ vs. ln $(T-T_m)$ plots at 1 kHz for the textured NK(N1-xSx)-CZ-BAZ piezoceramics: (a) x = 0.0, (b) x = 0.02, (c) x = 0.04, (d) x = 0.06, (e) x = 0.08, and (f) x = 0.1.

Table S3. T_m, T_{dev}, ΔT_m, and γ values of the textured NK($N_{1-x}S_x$)-CZ-BAZ piezoceramics ($0.0 \leq x \leq 0.10$)

x	T_m (°C)	T_{dev} (°C)	ΔT_m (°C)	γ
0.00	377	337	0	1.21699
0.02	291	295	4	1.34167
0.04	249	256	7	1.49983
0.06	179	188	9	1.60389
0.08	131	142	11	1.78439
0.10	69	82	13	1.91596

8. *P-E* and bipolar *S-E* curves of the textured NK($N_{1-x}S_x$)-CZ-BAZ piezoceramics

Fig. S8(a)–(g) show the *P-E* hysteresis curves of the textured NK($N_{1-x}S_x$)-CZ-BAZ piezoceramics ($0.01 \leq x \leq 0.09$). The textured x = 0.0 sample exhibited large P_S, P_r, and E_C values of 24.2 μC/cm, 22.7 μC/cm, and 0.99 kV/mm, respectively (Fig. S8(a)). The E_C value continuously decreased with an increasing x. The $0.01 \leq x \leq 0.06$ samples maintained large P_S and P_r values, which can be explained by the formation of the *R-O-T* mixed structures. However, the P_S and P_r values decreased when x exceeded 0.07, and the x = 0.1 sample exhibited very small P_S and P_r values because of the existence of the *C* (or pseudocubic) structure.

Fig. S8(a)–(g) show the bipolar *S-E* curves of the textured samples. The textured x = 0.01 sample exhibited a typical bipolar *S-E* curve with an S_{pos} value of 0.147 % (Fig. S8(a)), and the variation in the S_{pos} value was not significant. The x = 0.09 sample also exhibited a comparatively large S_{pos} of 0.161 % (Fig. S8(g)) owing to the large electrostriction effect. The S_{neg} value of the x = 0.01 sample was approximately 0.085% (Fig. S8(a)). The S_{neg} value increased with an increasing x, which started decreasing when x exceeded 0.04 and it was almost zero for the x = 0.09 sample. Because the x = 0.01 sample has normal ferroelectric properties, it has micron-size domains, leading to a relatively small S_{neg} (approximately 0.085%). As x increased, the textured samples exhibited an *R-O-T* mixed structure. Therefore, the $0.02 \leq x \leq 0.06$ samples have nanodomains that result in a large S_{neg} value. Moreover, the $x \geq 0.08$ sample exhibited a S_{neg} value close to zero owing to the presence of PNRs and their relaxor properties.

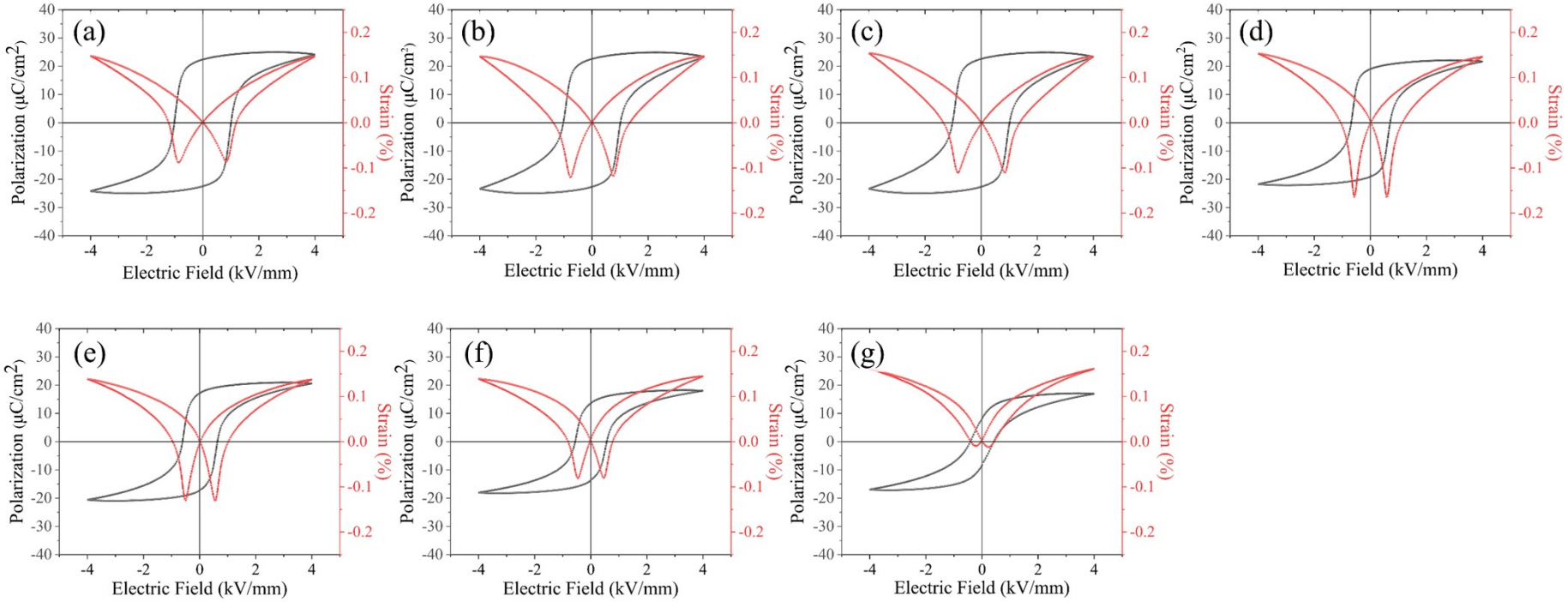

Fig. S8 *P-E* hysteresis and bipolar *S-E* curves of the textured NK($N_{1-x}S_x$)-CZ-BAZ piezoceramics: (a) x = 0.01, (b) x = 0.02, (c) x = 0.03, (d) x = 0.05, (e) x = 0.06, (f) x = 0.07, and (g) x = 0.09.

9. $\varepsilon^{T}_{33}/\varepsilon_0$ versus temperature curves for the textured NK($N_{1-x}S_x$)-CZ-BAZ piezoceramics

Fig. S9(a)–(f) show the $\varepsilon^{T}_{33}/\varepsilon_0$ versus temperature curves for the textured NK($N_{1-x}S_x$)-CZ-BAZ compositions ($0.0 \leq x \leq 0.1$), and the inset of each figure shows the variation in $\varepsilon^{T}_{33}/\varepsilon_0$ as a function of the temperature of the equivalent composition in a large temperature range of -50–400 °C. The T_C of the x = 0.0 composition was roughly 337 °C (Fig. S9(a)), and it decreased to 69 °C with an increasing x for the x = 0.1 composition (Fig. S9(f)), indicating that the T_Cs of the [001]-textured samples were similar to those of the untextured samples. The T_{O-T} decreased and the T_{R-O} increased with an increasing x, and they merged as T_{R-O-T} at approximately 45 °C in the x = 0.06 composition (Fig. S9(d)). Therefore, the behaviors of the T_{O-T} and T_{R-O} peaks of the textured samples were similar to those of the untextured samples. Additionally, the T_C and T_{O-T} (or T_{R-O-T}) peaks widened with an increasing x. Furthermore, the T_C and T_{O-T} (or T_{R-O-T}) peaks shifted to high temperatures with an increasing frequency and the difference in the temperature (ΔT) between the maximum and minimum frequencies increased with an increasing x. Therefore, the relaxor properties increased with an increasing Sb^{5+} content and the untextured samples exhibited identical results, as shown in Fig. S3(a)–(e). Therefore, it can be concluded that the $\varepsilon^{T}_{33}/\varepsilon_0$ versus temperature curves of the textured NK($N_{1-x}S_x$)-CZ-BAZ compositions ($0.0 \leq x \leq 0.1$) were identical to those of the untextured compositions.

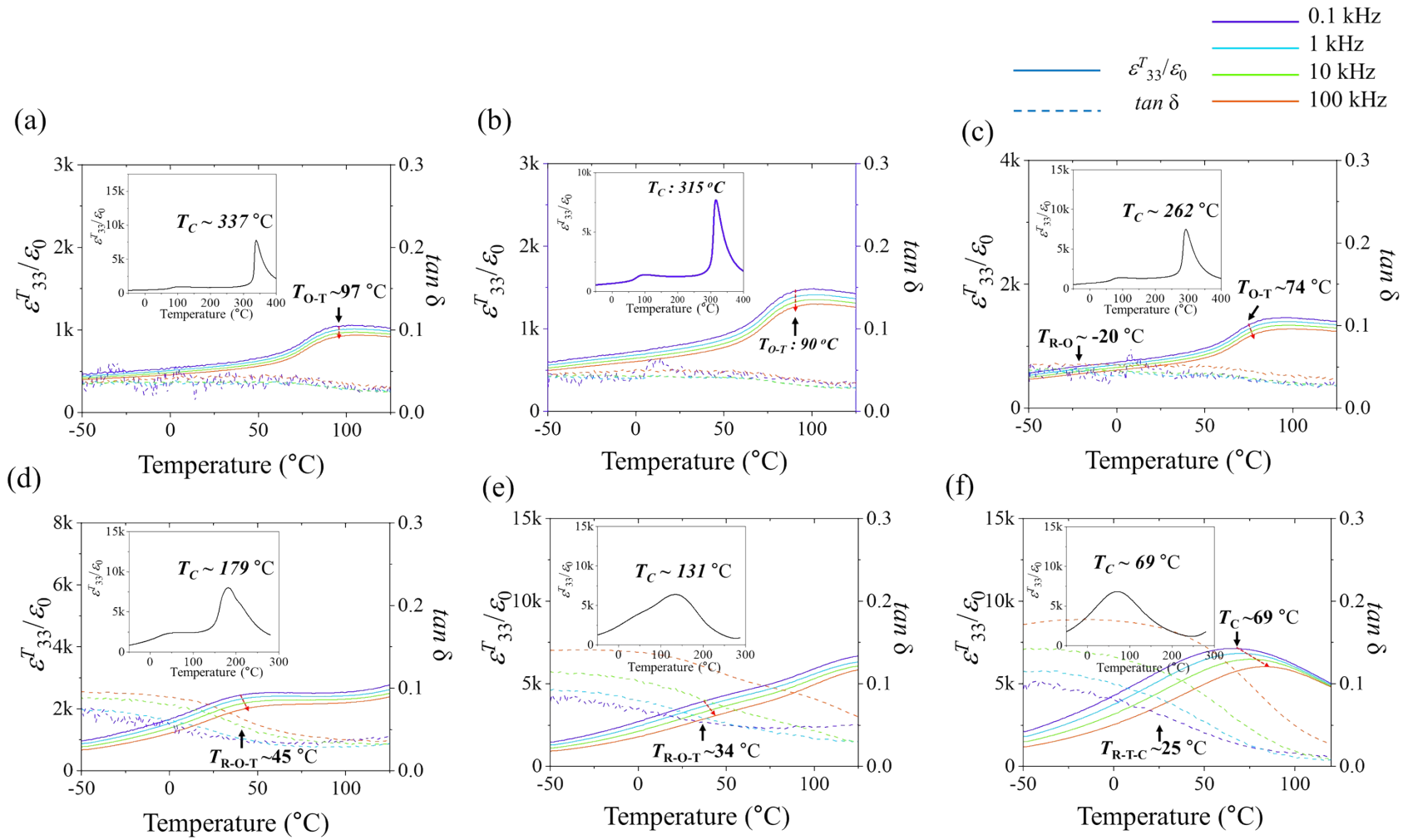

Fig. S9 $\varepsilon^T_{33}/\varepsilon_0$ versus temperature loops of the [001]-textured NK($N_{1-x}S_x$)-CZ-BAZ compositions with (a) x = 0.0, (b) x = 0.01, (c) x = 0.03, (d) x = 0.06, (e) x = 0.08, and (f) x = 0.1.

10. Strains of [001]-textured and untextured NK($N_{1-x}S_x$)-CZ-BAZ piezoceramics

The strain increased after [001]-texturing because the microstructure of the textured piezoceramic was similar to that of the single crystal grown along the [001] direction. According to previous studies [7-9] on NKN-based piezoceramics with an *R*-*O*-*T* structure, strain improvement is significant when the proportion of the *R*-*O* structure is greater than 80%, whereas strain improvement is comparatively small when proportion of the *R*-*O* structure is less than 80%. [7-9]. Fig. S10 shows the strains of the [001]-textured and untextured NK($N_{1-x}S_x$)-CZ-BAZ piezoceramics ($0.0 \leq x \leq 0.1$). Strain is observed to increase after [001]-texturing. Strain enhancement is significant for piezoceramics with $x \leq 0.05$ but it is relatively small for piezoceramic specimens with $x > 0.05$. For the NK($N_{1-x}S_x$)-CZ-BAZ piezoceramics ($0.0 \leq x \leq 0.05$), the proportion of the *R*-*O* structure is greater than 80%, indicating that the significant increase in strain after [001]-texturing can be attributed to the presence of a significant amount of *R*-*O* structure. For the piezoceramics with $x > 0.05$, the small strain enhancement could be attributed to the presence of a small amount of *R*-*O* structures.

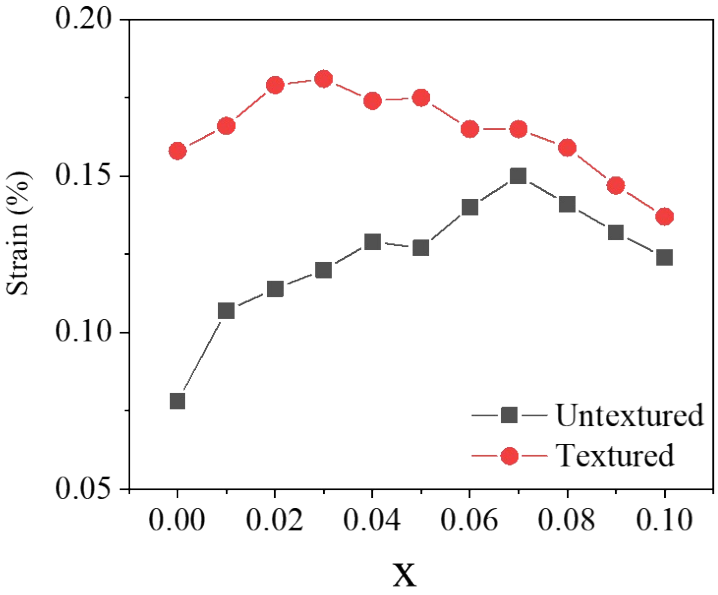

Fig. S10 Strains of the [001]-textured and untextured NK($N_{1-x}S_x$)-CZ-BAZ piezoceramics ($0.0 \leq x \leq 0.1$) obtained at 4.0 kV/mm.

11. Temperature-dependence of piezoelectrictricity of [001]-textured NK($N_{0.99}S_{0.01}$)-CZ-BAZ ceramic and output properties of the harvester measured at various accelarations

The d_{33} and k_p values of the [001]-textured NK($N_{0.99}S_{0.01}$)-CZ-BAZ piezoceramic (x = 0.01) were measured at different temperatures to evaluate its temperature stability. Fig. S11(a) shows the d_{33} values of the textured piezoceramics (x = 0.01) measured at various temperatures. The d_{33} value is 480 pC/N at 25 °C and does not vary significantly up to 100 °C. When the measuring temperature exceeds 100 °C, the d_{33} value decreases slightly with an increase in the measuring temperature; however, a relatively large d_{33} of 420 pC/N is maintained at 200 °C. Moreover, the d_{33} value at 295 °C is also high at 340 pC/N, but decreases considerably at temperatures exceeding 300 °C because the T_C of this piezoceramic is approximately 315 °C.

The k_p values of this piezoceramic (x = 0.01) measured at various temperatures are shown in Fig. S11(b). The k_p value is approximately 0.73 at 25 °C and is maintained up to 85 °C. When the measuring temperature exceeds 85 °C, the k_p value decreases to 0.51 and is maintained up to 220 °C. Because the $T_{O\text{-}T}$ of this piezoceramic is approximately 90 °C, $\varepsilon^T_{33}/\varepsilon_0$ increases slightly near 90 °C. Therefore, the decrease in k_p near 90 °C can be attributed to the increase in $\varepsilon^T_{33}/\varepsilon_0$ because k_p is inversely proportional to $(\varepsilon^T_{33}/\varepsilon_0)^{1/2}$. Although the k_p value decreases slightly when the measuring temperature exceeds 200 °C, a comparatively large k_p value of 0.41 is maintained up to 300 °C. Finally, the k_p value becomes zero near T_C, as shown in Fig. S11(b).

The V_{rms} of the piezoelectric energy harvester produced using the [001]-textured NK($N_{0.99}S_{0.01}$)-CZ-BAZ piezoceramic was measured at resonance frequency under an acceleration of 2.0 g, as shown in Fig. S11(c). V_{rms} increased with an increasing R_L and the largest V_{rms} of 63.58 V at an R_L of 0.91 MΩ. The I_{out}s generated by the harvesters were calculated using V_{rms}s, as shown in Fig. S11(d), and the harvester exhibited a largest I_{out} of 214 μA at 1.0 kΩ. The V_{rms}s of the harvesters were also measured at f_{off} of 250 Hz under the

acceleration of 2.0 g and the change in V_{rms} as a function of R_L is shown in Fig. S11(e). The V_{rms} of the harvester was small at low R_L values and increased with an increasing R_L and the largest V_{rms} of 535.5 mV at 1.0 MΩ. Fig. S11(f) provides the I_{out} with respect to R_L calculated using the V_{rms}s at 250 Hz. The applied acceleration is 2.0 g and the largest I_{out} of 2.41 μA at 1.0 kΩ.

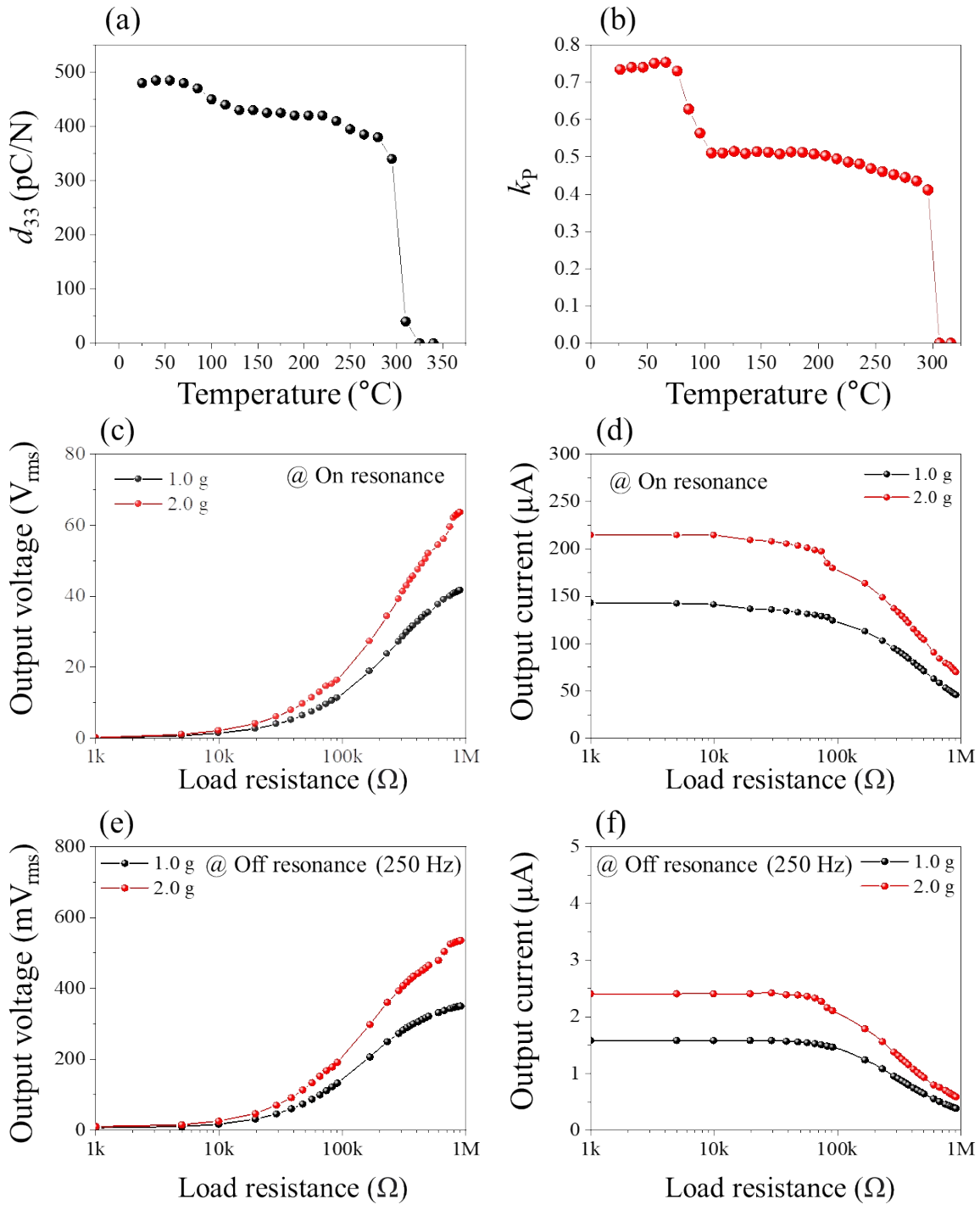

Fig. S11 (a) d_{33} and (b) k_p values of the [001]-textured NK($N_{0.99}S_{0.01}$)-CZ-BAZ piezoceramic measured at different temperatures. (c) V_{rms} versus R_L curves and (d) I_{out} versus R_L curves obtained at f_R under the accelerations of 1.0 g and 2.0 g. (e) V_{rms} versus R_L curves, and (f) I_{out} versus R_L curves obtained at f_{off} of 250 Hz under the accelerations of 1.0 g and 2.0 g.

References

[1] Y. Yan, D. Liu, W. Zhao, H. Zhou, H. Fang, Topochemical synthesis of a high-aspect-ratio platelet $NaNbO_3$ template, J. Am. Ceram. Soc., 2007, **90** 2399–2403.

[2] Y. Chang, Z. Yang, X. Chao, Z. Liu, Z. Wang, Synthesis and morphology of anisotropic $NaNbO_3$ seed crystals, Mater. Chem. Phys., 2008 **111**, 195–200.

[3] H.-Y. Park, K.-H. Cho, D.-S. Paik, S. Nahm, H.-G. Lee, D.-H. Kim, Microstructure and piezoelectric properties of lead-free $(1-x)(Na_{0.5}K_{0.5})NbO_3$-$xCaTiO_3$ ceramics, J. Appl. Phys., 2007, **102**, 124101.

[4] N. Setter, L.E. Cross, The role of B-site cation disorder in diffuse phase transition behavior of perovskite ferroelectrics, J. Appl. Phys., 1980, **51**, 4356–4360.

[5] M. Kuwabara, S. Takahashi, K. Goda, K. Oshima, K. Watanabe, Continuity in phase transition behavior between normal and diffuse phase transitions in complex perovskite compounds, Jpn. J. Appl. Phys., 1992, **31**, 3241.

[6] K. Uchino, S. Nomura, Critical exponents of the dielectric constants in diffused-phase-transition crystals, Ferroelectrics. 1982, **44**, 55–61.

[7] S.-H. Go, H Kim, D.-S. Kim, J.-M. Eum, S.-J. Chae, E.-J. Kim, S. Nahm, Improvement of piezoelectricity of (Na, K) Nb-based lead-free piezoceramics using [001]-texturing for piezoelectric energy harvesters and actuators, J. Eur. Ceram. Soc., 2022, **42**, 6478–6492.

[8] Y.-G. Chae, S.-J. Chae, S.-H. Go, E.-J. Kim, S.-J. Park, H. Song, S. Nahm, Ultrahigh Performance Piezoelectric Energy Harvester Using Lead-Free Piezoceramics with Large Electromechanical Coupling Factor, Int. J. Energy Res., 2023, **2023,** 20.

[9] S.-H. Go, D.-S. Kim, Y.-G. Chae, S.-J. Chae, E.-J. Kim, H.-M. Yu, B.-J. Kim, S.-J. Park, J.-H. Lee, S. Nahm, Effect of the Crystal Structure on the Piezoelectricity of [001]-Textured (Na, K)(Nb, Sb)O_3-$SrZrO_3$-(Bi, Ag)ZrO_3 Lead-Free Piezoelectric Thick Film. Actuators. 2023, **12**, 66.